AIAA-2000-2060

MIXING LAYER CHARACTERISTICS OF COAXIAL SUPERSONIC JETS

Erina Murakami*
Dimitri Papamoschou†
Department of Mechanical and Aerospace Engineering
University of California, Irvine
Irvine, CA 92697-3975

We present experimental results on mean flow development and mixing layer characteristics of single and dual-stream compressible air jets. The results are relevant to noise emission and mixing enhancement of high-speed turbulent jets. In the dual-stream jets, the primary flow was fixed at Mach number 1.5 and the secondary stream was supplied at various subsonic Mach numbers and from a variety of nozzles. Coaxial and eccentric nozzle configurations were investigated. In the coaxial arrangements, the secondary flow reduces the growth rate of the primary shear layer and elongates the primary potential core and the supersonic region of the jet. As a result, the entrainment rate of the coaxial jet is less than that of the single jet. The potential core length increases by as much as 68% when a thick secondary stream is supplied at Mach number 0.9. The eccentric configuration shows substantial improvement in mixing over the coaxial case and achieves an entrainment rate comparable to that of the single jet when the thickness of the secondary flow is relatively small. In the eccentric case, the maximum observed elongation of the primary potential core was 20% relative to the single jet case. An empirical model for predicting the primary and secondary potential core lengths of a coaxial jet is proposed.

INTRODUCTION

Motivation

Noise radiated from supersonic jets is a serious environmental problem whose solution has challenged engineers and scientists for more than four decades. A review of various silencing techniques for high-speed jets can be found in Seiner and Kresza [1]. Recents works have called attention to the substantial noise reduction achievable by utilizing a secondary stream to reduce noise production from the primary flow. Example is the Mach Wave Elimination (MWE) technique, where a secondary flow prevents formation of Mach waves from the primary jet [2]. Key elements of successful implementation of MWE are the length of the Mach wave emitting region of the jet and the ability of the secondary flow to cover that region. If coverage is incomplete, substantial Mach wave emission still occurs. In the initial implementations of MWE, the secondary flow was supplied by an annular nozzle around the primary jet. A major drawback of the coaxial arrangement is that the secondary flow reduces the growth rate of the primary jet, hence lengthens the Mach wave emitting region of the jet. As a result, thick secondary flows were required to cover the dominant noise-source region and achieve appreciable noise reduction. This drawback was circumvented by supplying the secondary flow from an eccentric nozzle [3]. The eccentric arrangement yielded a growth rate comparable to that of the single jet and directed the benefit of the secondary flow in the downward direction, which is most pertinent to community noise. Figure 1 shows Mach wave emission from a single jet, a coaxial jet, and an eccentric jet, all of them sharing the same primary flow and the latter two sharing the same secondary-flow velocity, Mach number,

*Graduate Student, member AIAA
†Professor, senior member AIAA

and mass flow rate. Application of an annular secondary flow eliminates the near-field Mach waves but some far-field Mach waves are still present. In the eccentric case, the lower hemisphere is devoid of Mach waves, while radiation is unaltered in the upper hemisphere. The resulting downward noise reduction is vastly superior to that obtained by the equivalent coaxial arrangement, as illustrated by the spectra of Fig. 2.

Although the immediate motivation for this work is refinement of the MWE method, our study is generic enough to impact mixing and noise emission from a wide variety of high-speed, dual-stream jets. Our fundamental interest is the effect of the secondary flow on the development of the primary flow in coaxial and eccentric nozzles. Specifically, we study the shear layer growth rate, the length of the potential core, and the extent of the supersonic region of the jet. The region around the primary potential core is the region of the dominant noise sources [4]. Knowing how this region scales with flow parameters is extremely important for noise prediction.

Dual-stream jets, especially in coaxial configurations, are found in a large variety of practical devices such as engine exhausts and fuel injectors. Early works on coaxial jets were motivated mainly by applications in combustion and aircraft propulsion. Forstall and Shapiro [5] conducted an experimental investigation on mass and momentum transfer between the two streams of a coflowing jet with very large secondary flows. They determined that the velocity ratio of the primary to secondary stream is the principal variable determining the shape of the mixing region. An empirical relation for the length of the primary potential core was proposed. Other works in subsonic, axisymmetric, turbulent coaxial jets have studied the near-field region at various velocity ratios. Ko and Kwan [6], Champagne and Wygnanski [7], Durao and Whitelaw [8], and Gladnick et al. [9] investigated the development of the flow field and its approach to a self-preserving state. These studies conclude that the instability and flow development depend on the velocity and density ratios across the shear layers. Williams et al. [10] investigated the flow structure and acoustics of subsonic coaxial jets and suggested a method of predicting the noise attenuation when the jet is surrounded by an annular flow of variable velocity.

Only a handful of investigations have encompassed coaxial jets with a supersonic primary flow. Eggers and Torrence [11] obtained data on turbulent mixing for a supersonic coaxial air jet with the secondary

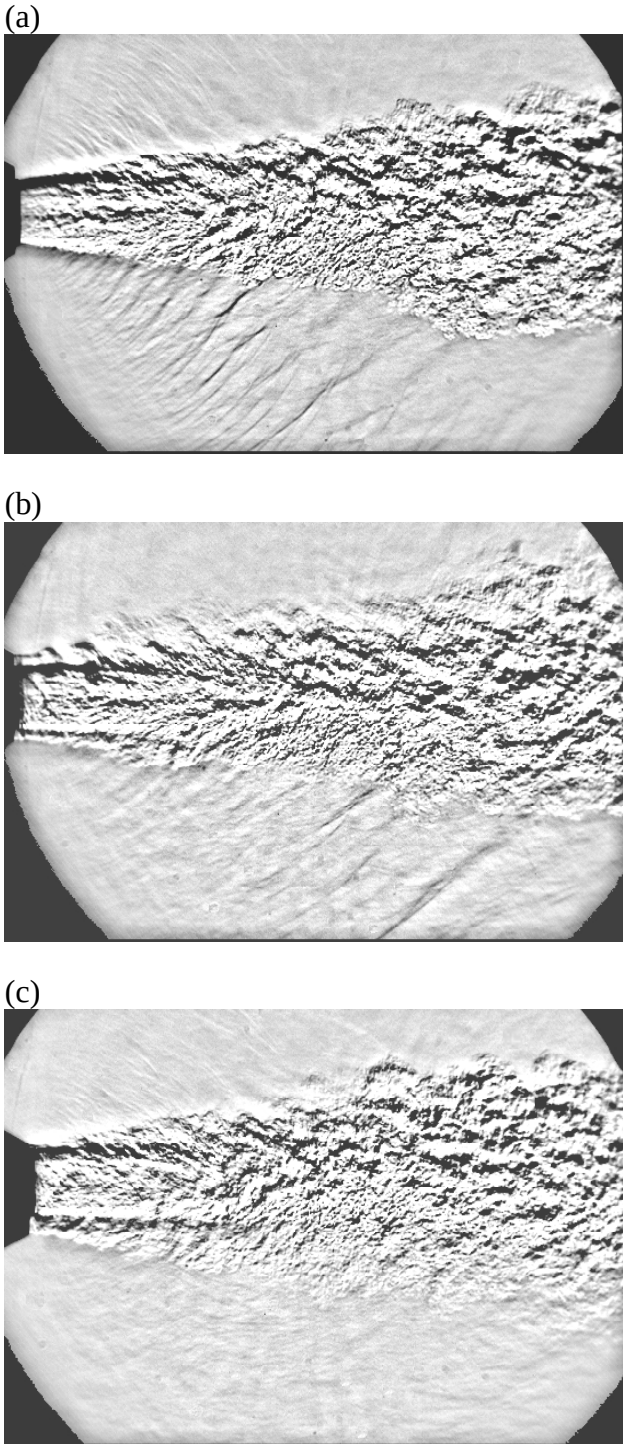

Fig.1 Spark schlieren images of Mach wave radiation from a jet with Mach number 1.5 and velocity 700 m/s. (a) Single jet; (b) jet surrounded by an annular coflow with velocity of 350 m/s; (c) jet surrounded by an eccentric coflow with velocity of 350 m/s [3].

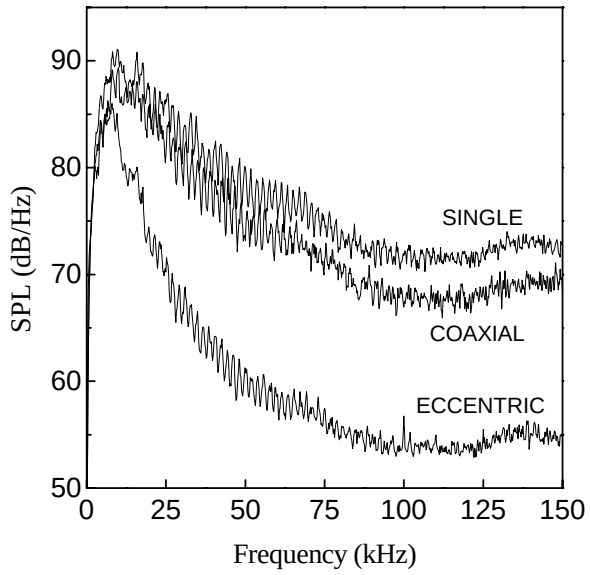

Fig.2 Far field noise spectra in the direction of peak downward emission for the single, coaxial, and eccentric jets shown in Fig. 1

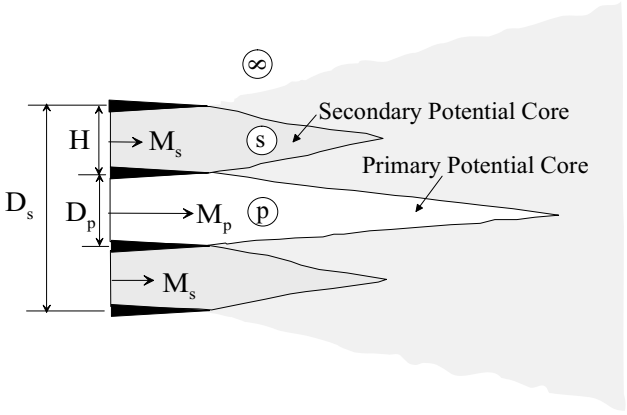

Fig.3 Coaxial jet configuration.

stream having a larger velocity than the primary stream (inverted velocity profile). Schadow et al. [12] made spreading rate measurements in a coaxial jet with normal velocity profile and determined that the effect of compressibility on the growth rate was very similar to that measured in planar shear layers. Although these studies provide useful insight into the flow characteristics of coaxial jets, there has been no systematic study on the effects of velocity, Mach number, and thickness of the secondary flow on the mean flow development of coaxial jets. The primary objective of our study is to develop scaling laws for the extent of the noise-source region of single and dual-stream, high-speed jets. It was deemed important to include not only the conventional coaxial arrangement but also the eccentric arrangement which proved so beneficial in reducing Mach wave emission. We chose cold air jets because of the ease by which one can compute velocity and density profiles from pitot pressure surveys. However, the models proposed here are general enough to be used with hot or variable-composition jets.

Planar shear layer model

The near field of a dual-stream jet consists of two shear layers, one between the primary and secondary flows, and the other between the secondary flow and the ambient air, as illustrated in Fig. 3. Each shear layer is similar to a planar shear layer as long as the thickness is small compared to the radius of the potential core that it surrounds. It is thus important to review the planar shear layer relations because they will prove very helpful in developing models for the potential core lengths of the coaxial jet.

Considering a shear layer between a fast and a slow stream, its growth rate can be expressed as [13]

$$\delta' = \delta'_0(r,s) f(M_c) \tag{1}$$

where

$$\delta'_0 = C\frac{(1-r)(1+\sqrt{s})}{1+r\sqrt{s}} \tag{2}$$

is the growth rate of the equivalent incompressible shear layer, with $r = U_{\text{slow}}/U_{\text{fast}}$, $s = \rho_{\text{slow}}/\rho_{\text{fast}}$ and C a constant that depends on the definition of layer thickness. $f(M_c)$ is a compressibility correction based on the convective Mach number

$$M_c = \frac{U_{\text{fast}} - U_{\text{slow}}}{a_{\text{fast}} + a_{\text{slow}}} \tag{3}$$

A curve fit through the growth rate data of various investigations [13, 14, 15, 16] gives the following

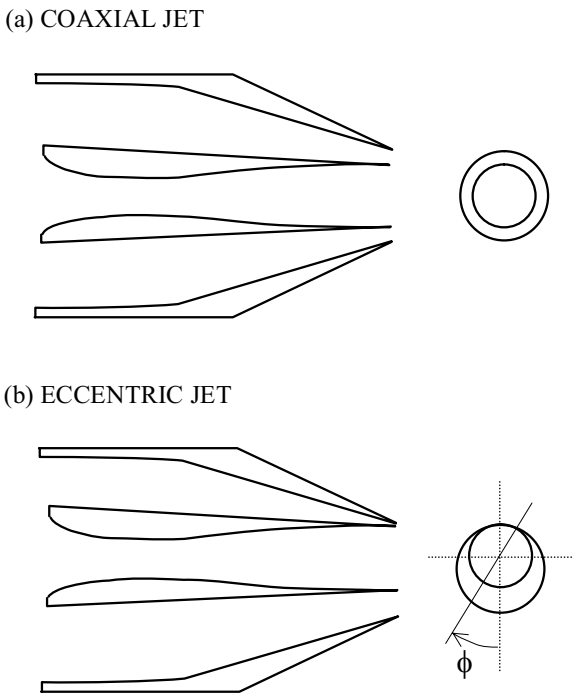

Fig.4 Nozzle configurations used in present study.

approximation of the compressibilty correction:

$$\frac{\delta'}{\delta'_0} = f(M_c) = 0.23 + 0.77e^{-3.5M_c^2} \qquad (4)$$

which describes the stabilizing effect of convective Mach number on the growth rate. For the growth rate of the pitot thickness (see Fig. 5), Papamoschou and Roshko [13] determined the constant in Eq. 2 to be $C = 0.14$.

EXPERIMENTAL PROGRAM

Experiments were conducted in an a dual-stream jet facility described in several earlier publications [2, 3]. Figure 4 shows the nozzle arrangements used in this study. Coaxial and and eccentric nozzle configurations were derived from the same assembly, with the eccentric jet having the inner nozzle offset to touch the outer nozzle. Air at room reservoir conditions was supplied to the primary and secondary nozzles. The primary (inner) nozzle of exit diameter $D_p = 12.7$ mm was designed by the method of characteristics for Mach number 1.5. The jet Reynolds number was 550,000. Three conical secondary (outer) nozzles were used, with exit diameters $D_p = 17.8$, 21.6 and 25.4 mm. The primary jet was perfectly expanded and the surrounding air was at ambient, still conditions. The secondary flow was naturally pressure-matched at subsonic conditions. Nozzle configurations and flow conditions are summarized in Tables 1 and 2. Table 3 lists the mass flow ratio $\dot{m}_s/\dot{m}_p$ and thrust ratio F_s/F_p for each flow-nozzle combination. For ease of reference we use a labeling system that describes the size and shape of the secondary nozzle and the Mach number of the secondary flow. Coaxial nozzles are denoted by Cxx and eccentric nozzles by Exx, where $xx = 10 \times D_s/D_p$. The secondary flow is denoted by Myy, where $yy = 100 \times M_s$. Case C20M37, for example, describes the coaxial jet with Mach 0.37 secondary flow exhausting from a coaxial arrangement with $D_s/D_p = 2.0$. Case E17M90 has a Mach 0.9 secondary stream supplied through an eccentric configuration with $D_s/D_p = 1.7$. The single Mach 1.5 jet is denoted SINGLE.

Table 1 Nozzle Configurations

Nozzle	D_s/D_p	Configuration
C14	1.4	Coaxial
C17	1.7	Coaxial
C20	2.0	Coaxial
E14	1.4	Eccentric
E17	2.0	Eccentric

Table 2 Flow conditions

Case	M_p	U_p (m/s)	$\frac{\rho_p}{\rho_\infty}$	M_s	U_s (m/s)	$\frac{\rho_s}{\rho_\infty}$
SINGLE	1.5	430	1.45	0	0	1.00
M37	1.5	430	1.45	0.37	130	1.03
M60	1.5	430	1.45	0.60	210	1.07
M90	1.5	430	1.45	0.90	290	1.16

Table 3 Mass Flow Rate and Thrust Ratios

Case	$\dot{m}_s/\dot{m}_p$	F_s/F_p
C14M37, E14M37	0.20	0.06
C14M60, E14M60	0.33	0.15
C14M90, E14M90	0.52	0.35
C17M37, E17M40	0.39	0.11
C17M60, E17M60	0.65	0.30
C17M90, E17M90	1.02	0.69
C20M37	0.62	0.18
C20M60	1.03	0.48
C20M90	1.62	1.09

Pressure transducers recorded the total pressures of the primary and secondary streams. Pitot probe

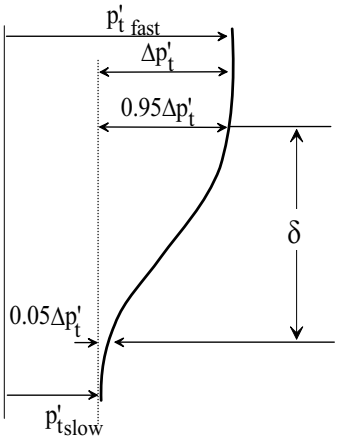

Fig.5 Definition of shear layer pitot thickness.

surveys were conducted at various downstream positions from the jet exit. The inlet of the pitot probe was flattened to an opening 0.25 mm high and 2.0 mm wide, giving a spatial resolution of about 0.25 mm. The probe was mounted on a carriage that traversed the jet plume at a controlled speed which ranged from 6 mm/s to 14 mm/s. The probe was connected to a pressure transducer (Setra Model 280) which was also mounted on the carriage to minimize the tubing length between the probe and the transducer. This arrangement reduced the response time of the probe-transducer low enough to resolve sharp gradients in the pitot pressure near the nozzle exit. Mach number, velocity, and density profiles were extracted from the pitot-pressure profiles under the assumptions of constant static pressure (equal to ambient) and constant total temperature (equal to room temperature). Pitot pressures as a function of radial position from the jet centerline were obtained at streamwise locations from $x/D_p = 0$ to 20. For the coaxial jets, it was sufficient to obtain profiles on a single plane passing through the jet axis. For the eccentric configurations, profiles were obtained on the azimuthal planes $\phi = 0°, 23°, 45°, 68°$, and $90°$. These intervals were fine enough to allow accurate interpolation for intermediate values of ϕ and to thus obtain the entire jet flowfield. The shear layer pitot thickness, δ', is the width of the pitot pressure profile from 5% to 95% of the difference in the free-stream values. This definition is illustrated in Fig. 5.

RESULTS AND DISCUSSION

Mean Flow Characteristics

Figure 6 presents the evolution of velocity profiles for the single jet. The primary potential core is outlined with dashed lines; its length is defined here as the distance from the jet exit to the location where the centerline velocity decays to 90% of the primary jet exit velocity. This definition applies to all the cases presented in this paper. For the single Mach 1.5 air jet, the potential core length is 9.2 jet diameters, or $L_p/D_p = 9.2$. Table 4 lists the measured potential core lengths and supersonic lengths, to be defined below, for all the cases covered.

Figure 7 presents the velocity profiles of coaxial jets with secondary flow issuing from nozzle C20. The presence of a secondary potential core is evident in the figures. The secondary potential core length is the distance from the jet exit to the location where the flat feature of the velocity profile, corresponding to the core of the secondary stream, can no longer be observed. The centerline velocity decays at an increasingly slower rate as the secondary Mach number increases. As a result, the primary potential core is elongated substantially relative to the SINGLE case. With $M_s = 0.9$, the potential core reaches $L_p/D_p = 15.5$, a 68% increase from the SINGLE case. The plots in Fig. 8 compare the velocity profiles of coaxial jets with the same secondary flow ($M_s = 0.9$) exhausting from secondary nozzles of different sizes. It is observed that the length of the primary potential core increases with thickness of the secondary flow.

When the secondary stream issues from an eccentric nozzle, the results are quite different from those of the coaxial configurations. Figure 9 shows velocity profiles surveyed on the azimuthal plane $\phi = 0°$. Compared to the coaxial case, the secondary flow on the lower side of the jet has twice the thickness and thus has a secondary potential core that is twice as long. The primary potential core length is shorter than in the coaxial case, and a minimal amount of lengthening is evident relative to the SINGLE case. For example, in the coaxial case C14M90, the potential core length was increased by 36% relative to the SINGLE case. With the corresponding eccentric configuration E14M90, the potential core length increases by only 10%. Similarly, the increase in primary potential core length with addition of the secondary stream in C17M90 is 64% whereas E17M90 yields a 18% increase.

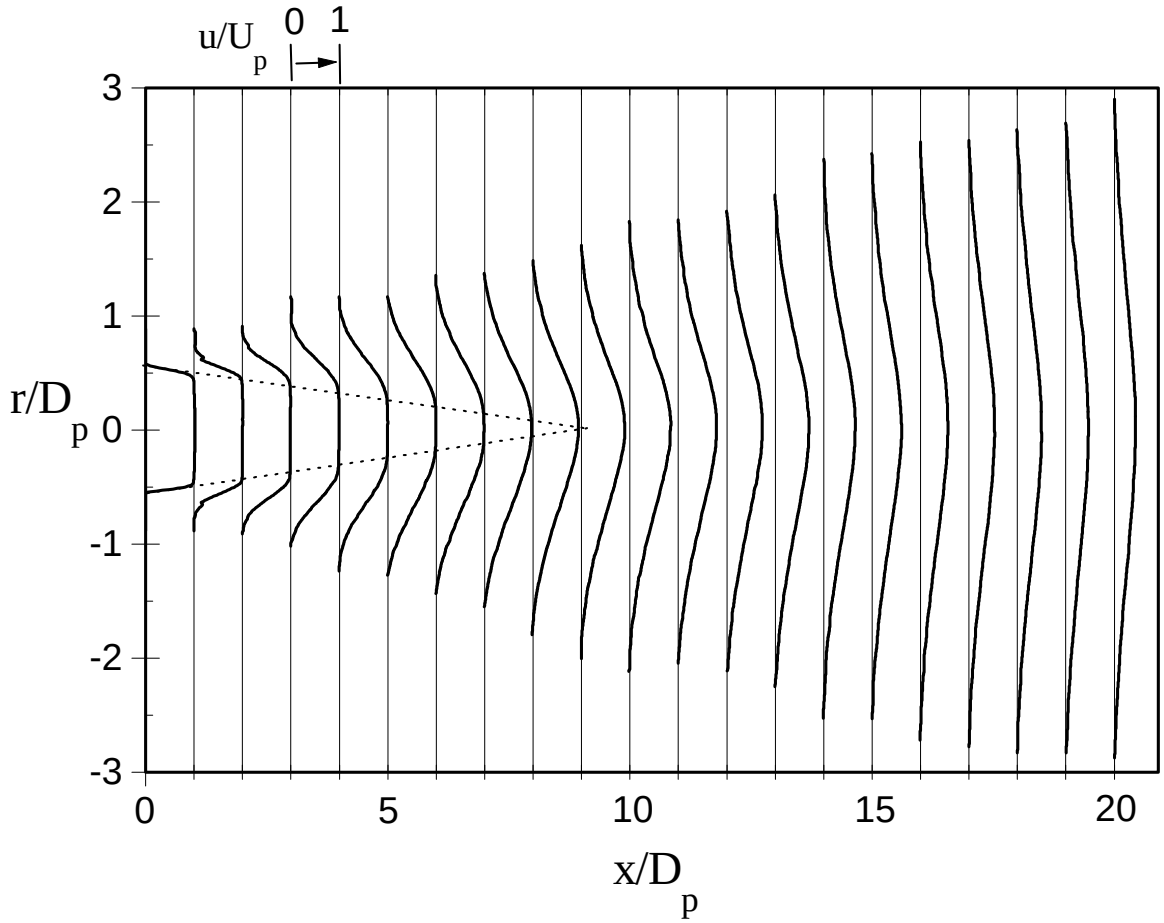

Fig.6 Normalized velocity profiles for case SINGLE.

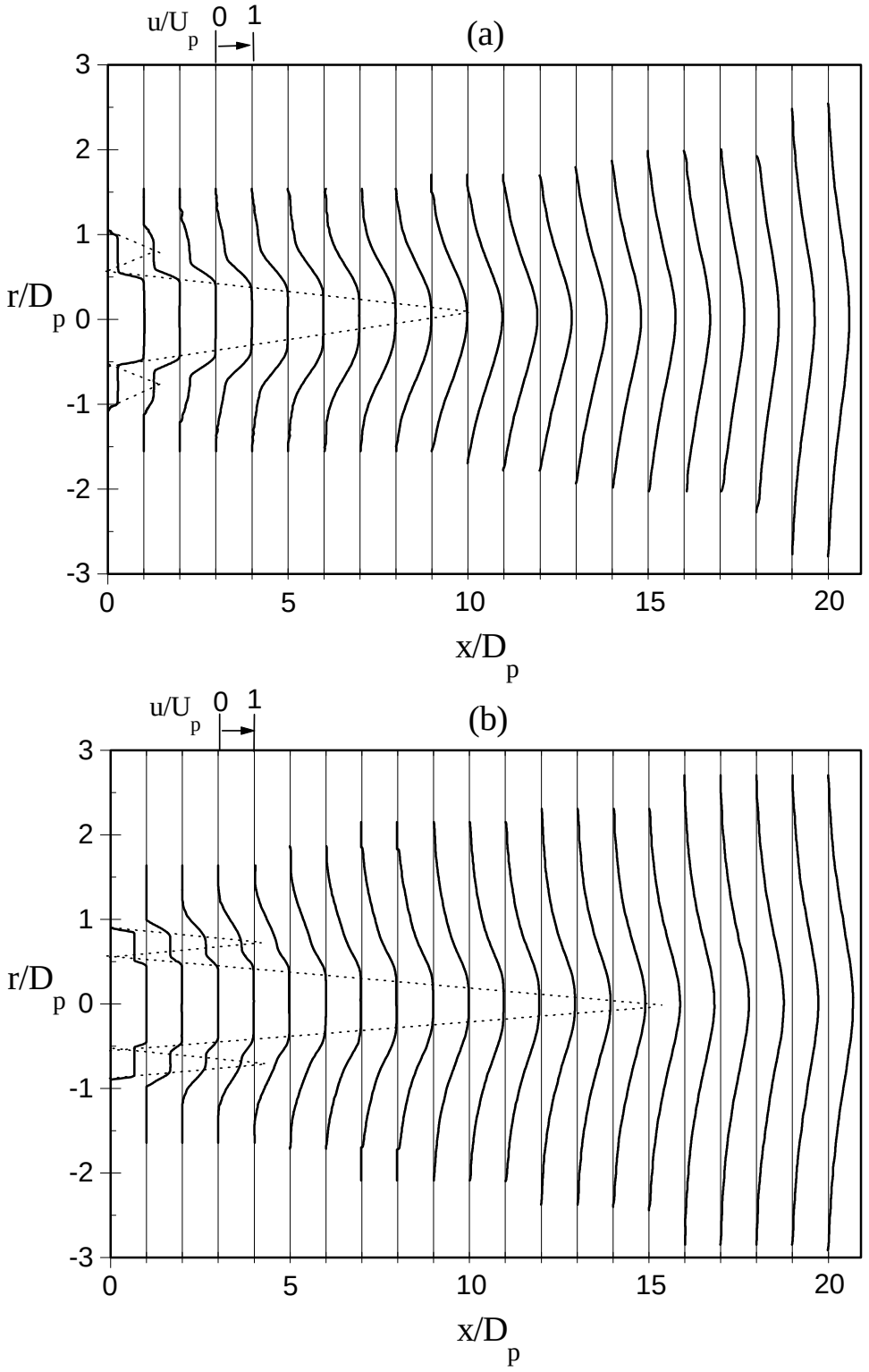

Fig.7 Normalized velocity profiles for coaxial jet cases (a) C20M37 and (b) C20M90.

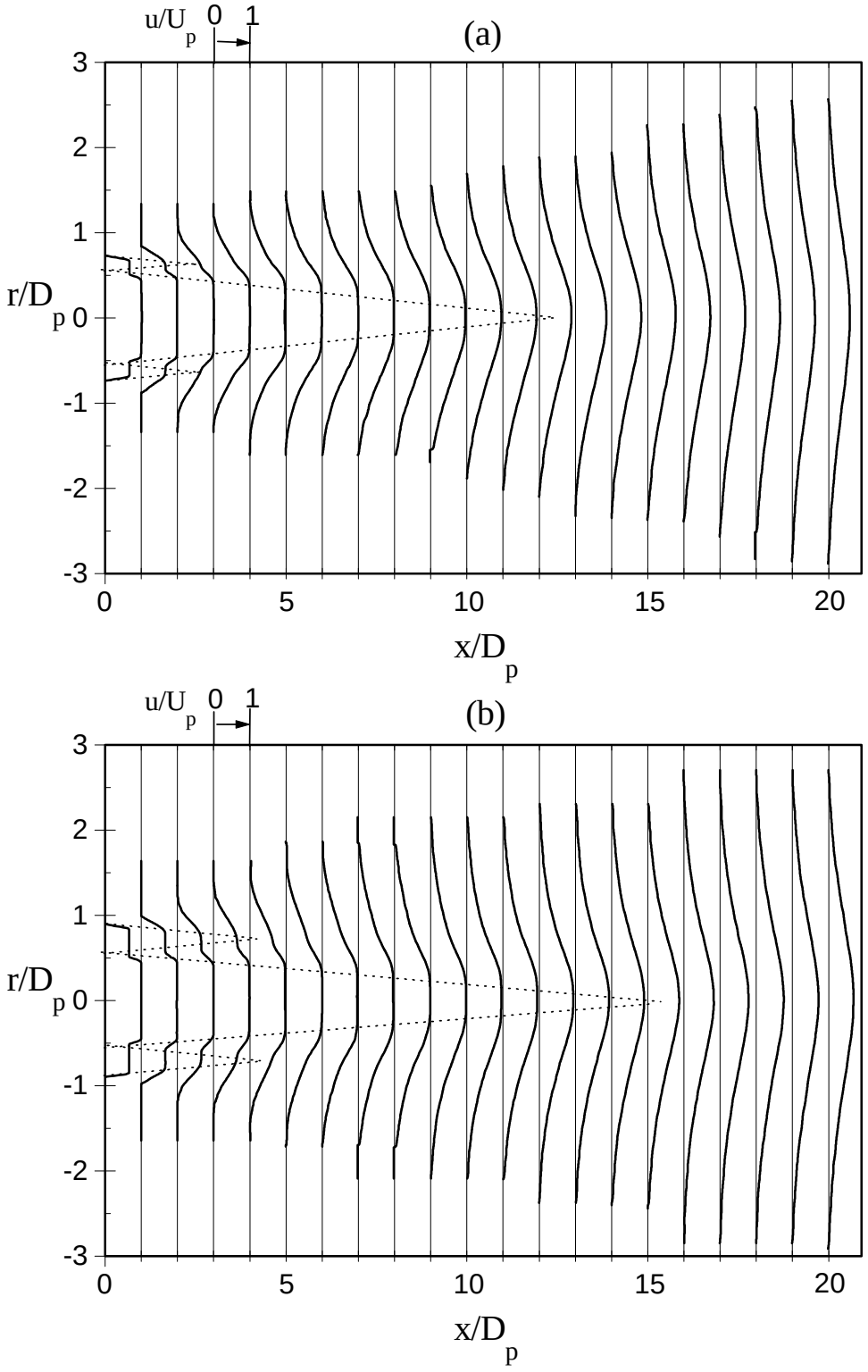

Fig.8 Normalized velocity profiles for coaxial jet cases (a) C14M90 and (b) C17M90.

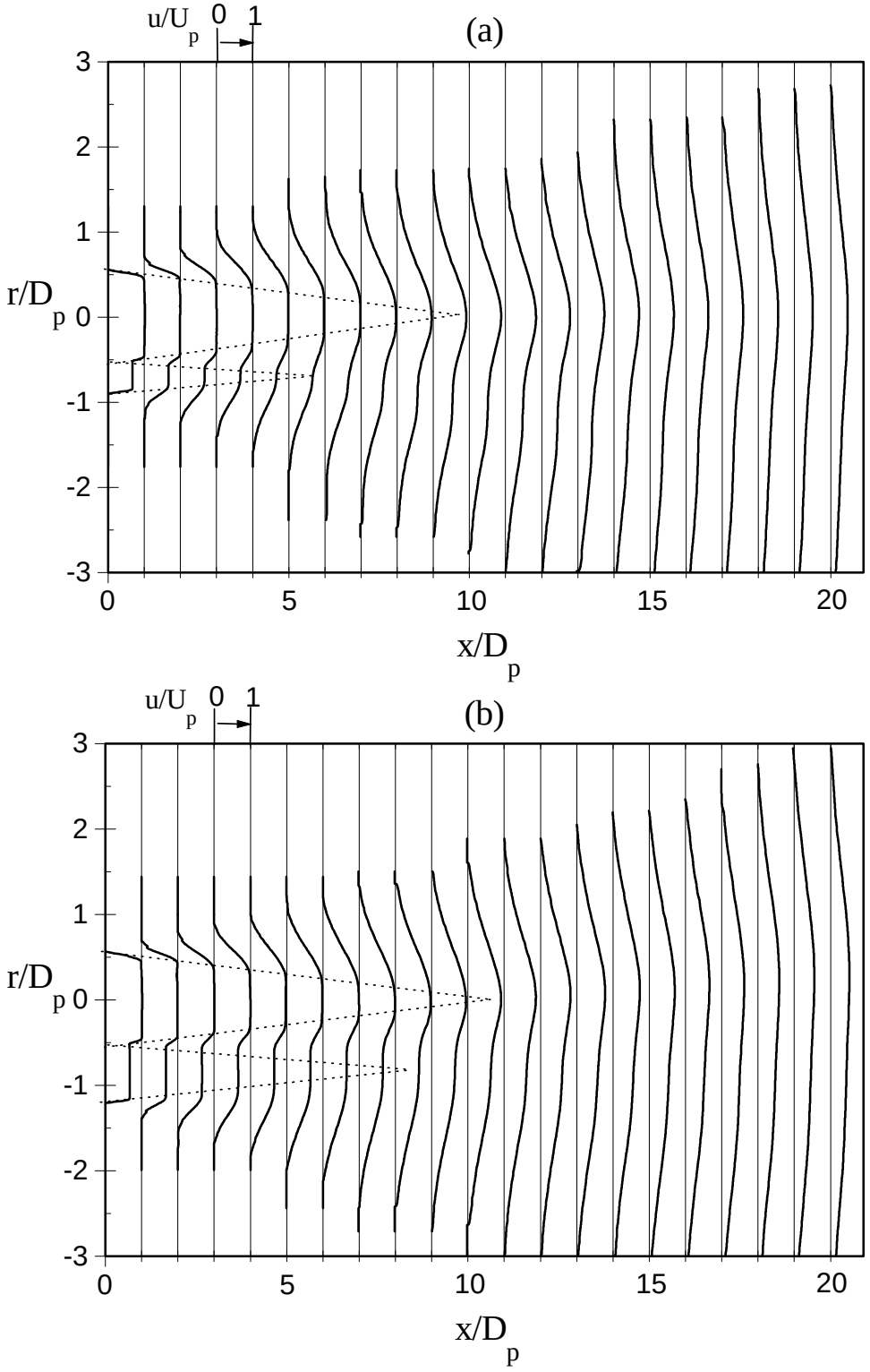

Fig.9 Normalized velocity profiles for eccentric jet cases (a) E14M90 and (b) E17M90.

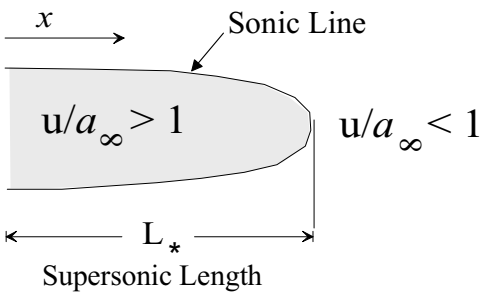

Fig.10 Definition of supersonic length L_*.

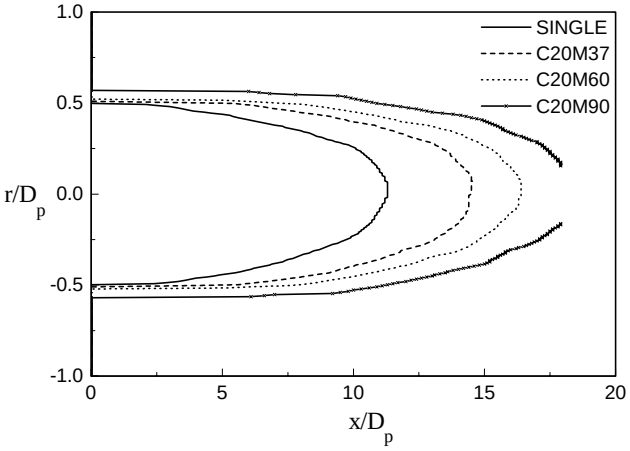

Fig.11 Sonic lines for SINGLE and coaxial jets with nozzle C20.

Besides the potential core, a region of relevance to high-speed jet noise is the extent of the flow that has supersonic motion relative to the surrounding medium, defined by $u/a_\infty > 1$. The supersonic region contains intense noise sources [4] such as Mach waves and, in the case of imperfectly-expanded jets, screech/broadband shock noise. To locate the supersonic region we trace the location of the sonic line $u/a_\infty = 1.0$ which separates the supersonic region from the subsonic one, as illustrated in Fig. 10. The length of the supersonic region is denoted by L_*. Sonic line contours are plotted in Fig. 11 for coaxial jets with the C20 secondary nozzle. It is seen that the supersonic region elongates with increasing secondary-flow Mach number. Figure 12(a) compares the sonic lines of the coaxial case C14M90, the eccentric case E14M90, and the SINGLE case. The coaxial jet has a supersonic region 31% longer than that of the SINGLE jet. In contrast, the supersonic region of the eccentric jet is only 6% longer than the supersonic region of the SINGLE jet. Similar trends are observed in the comparison of C17M90, E17M90, and SINGLE, shown in Fig. 12(b).

Comparing the supersonic lengths with the potential

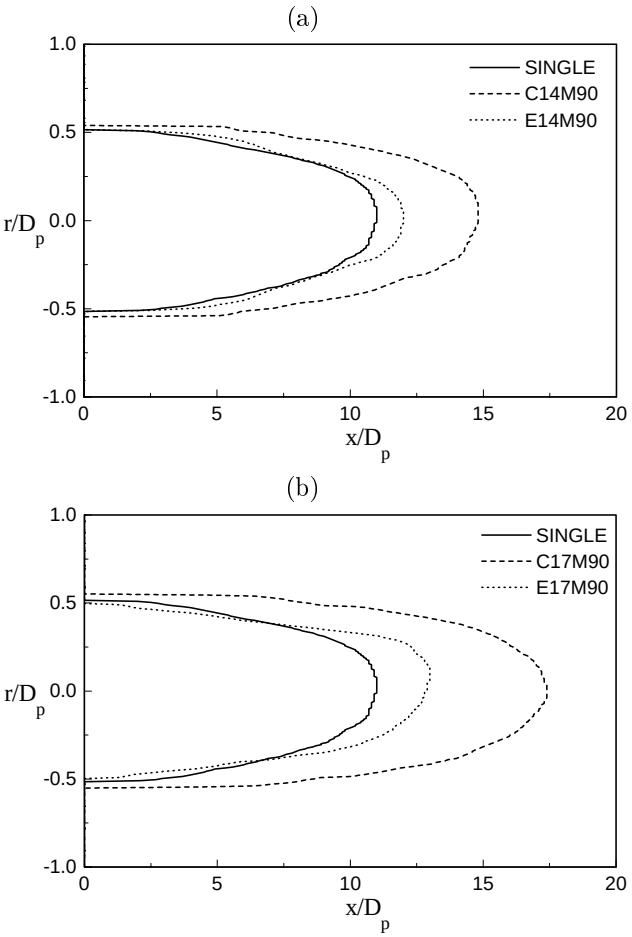

Fig.12 Sonic lines for coaxial and eccentric jets with comparison to SINGLE. (a) C14M90 and E14M90; (b) C17M90 and E17M90.

core lengths listed in Table 4, we note that the two are roughly proportional, $L_*/L_p \approx 1.2$. This ratio is close to the ratio U_p/a_∞=1.24, which suggests the relation $L_*/L_p \approx U_p/a_\infty$ for supersonic jets. At this point this is a preliminary observation that needs validation in higher- and lower-speed supersonic jets.

Table 4 Potential Core Lengths and Sonic Lengths

Case	L_s/D_p	L_p/D_p	L_*/D_p	L_*/L_p
SINGLE		9.2	11.3	1.23
C14M37	1.5	10.5	12.4	1.18
C14M60	2.0	11.4	13.5	1.18
C14M90	2.5	12.5	14.8	1.18
C17M37	3.0	11.4	13.4	1.18
C17M60	3.5	13.3	15.6	1.17
C17M90	4.0	15.1	17.4	1.15
C20M37	3.5	12.3	14.5	1.18
C20M60	4.5	13.8	16.4	1.19
C20M90	5.5	15.5	18.5	1.19
E14M37	2.5	9.8	11.5	1.17
E14M60	4.0	9.9	12.0	1.21
E14M90	5.5	10.1	12.0	1.19
E17M37	6.0	10.4	12.2	1.17
E17M60	7.0	10.7	12.7	1.19
E17M90	8.0	10.9	13.0	1.19

Mixing Characteristics

A quantitative measure of mixing is the mass flow rate of the jet plume

$$\dot{m} = \int_A \rho u dA \tag{5}$$

The mass flow rate was calculated from the velocity and density profiles obtained at each downstream station. In theory, integration should be performed over a very large area at the edges of which the velocity is practically zero. Since velocity profiles were available for a finite radial distance from the jet, the mass flow rate was obtained by carrying out the integration to a radial location at which the momentum flux (which is invariant in a zero-pressure-gradient jet) was 99% of the nozzle exit value. In other words, the integration area A was such that

$$\int_A \rho u^2 dA \; = \; 0.99F \tag{6}$$

where F is the total thrust measured at the nozzle exit.

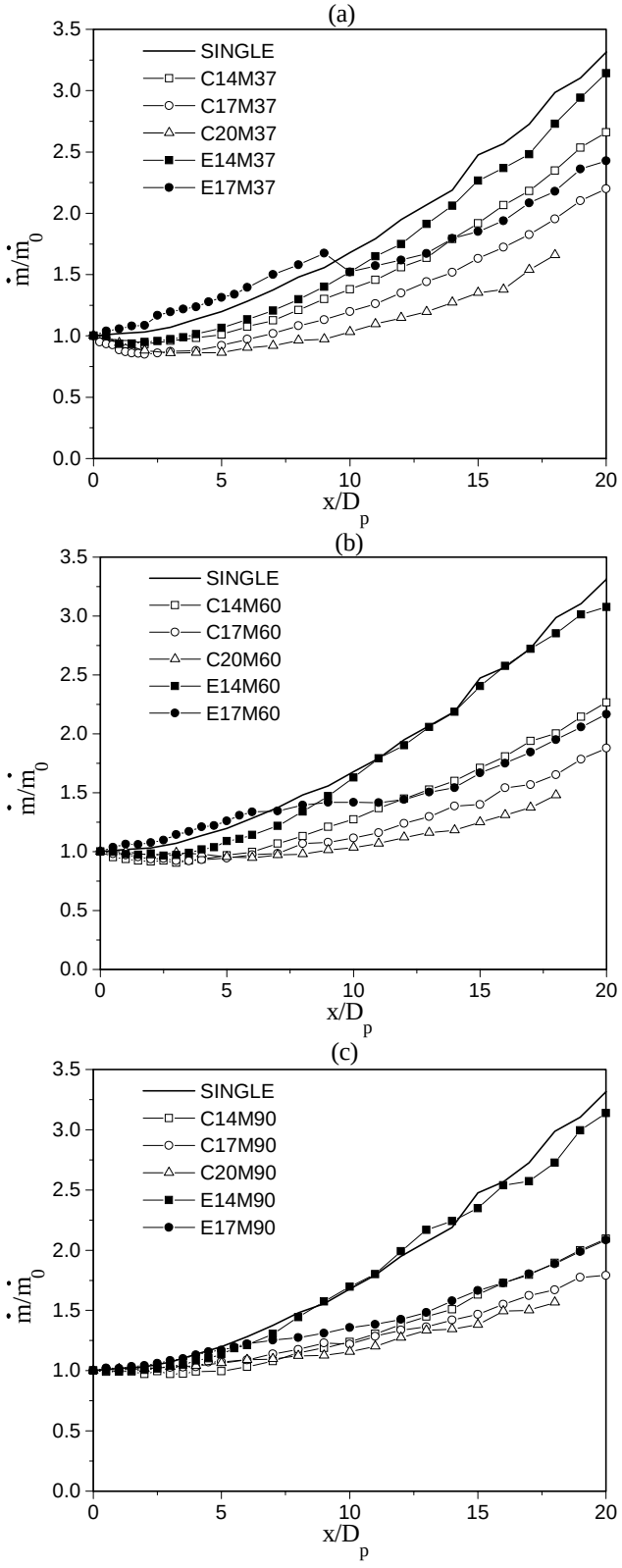

Fig.13 Normalized mass flow rates for jets with secondary flow conditions (a) M37; (b) M60; and (c) M90.

The mass flow rate was normalized by the nozzle exit value, $\dot{m}_0$, to obtain a measure of the entrainment rate of the jet. Figures 13(a), (b), and (c) plot $\dot{m}/\dot{m}_0$ versus axial distance for the flows M40, M60, and M90, respectively. Each plot also includes the mass flow rate of the SINGLE jet for comparison. The slight dip of the normalized flow rate near the nozzle exit is probably due to pressure non-uniformity which is not included in our calculation of mass flow rate and momentum flux.

For the coaxial configurations it is evident that increasing the secondary Mach number and/or increasing the size of the secondary nozzle results in a lower entrainment rate. When the same flow conditions are exhausted through an eccentric nozzle configuration, the entrainment rate increases relative to the coaxial configuration. This increase is substantial for the smaller eccentric nozzle E14, with the mass flow rates reaching values close to those of the single jet. With the larger nozzle E17, however, the increase relative to the coaxial configuration is moderate. It is interesting to note a strange occurrence with nozzle E17. The normalized mass flow rate increases rapidly with downstream distance and suddenly drops and assumes a slower growth rate that is close to the that of the coaxial case. This transition is more exaggerated with secondary flow M37 and occurs in each case before the end of the primary potential core.

By comparing coaxial cases with same secondary nozzles, it is noted that the largest entrainment rate occurs for the lowest secondary-flow Mach number. The growth rate of the primary jet is affected primarily by the velocity ratio U_p/U_s. Compressibility and density ratio also play significant roles but not as dominant as that of the velocity ratio. This trend, therefore, is not surprising.

Growth Rates

The growth rates of the primary and secondary shear layers, δ'_p and δ'_s, were measured in the near field of the jet. They are based on the pitot thickness defined in Fig. 5 and their values are listed in Table 5. The growth rate was determined from at least three pitot thickness data beginning from the upstream-most survey location, not including the one at the jet exit, to a location before the end of the secondary potential core. Typically, pitot profiles were obtained at $x/D_p = 0, 1, 2, \ldots$. For cases in which a short secondary potential was expected, particularly with nozzle C14, profiles were obtained at intermediate positions $x/D_p = 0.25, 0.5, 0.75, \ldots$. For a fully

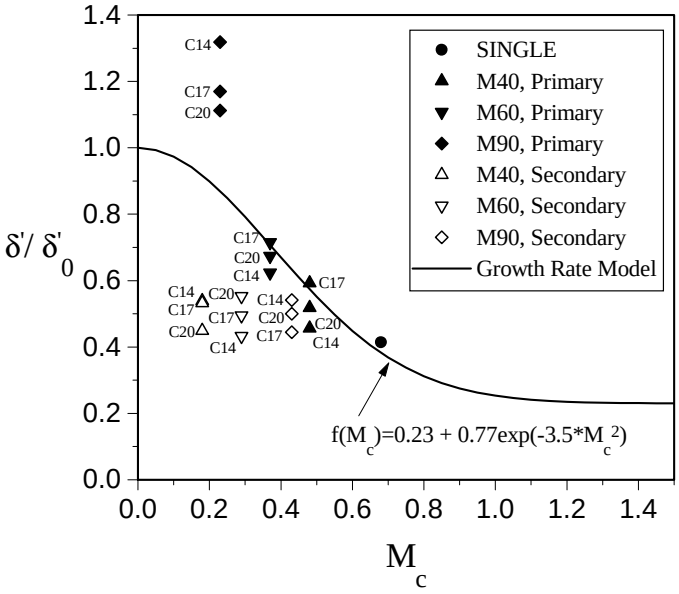

Fig.14 Normalized growth rates of the coaxial jet shear layers versus convective Mach number.

turbulent shear layer, the thickness grows linearly with downstream distance. The growth rate was obtained from a linear least-squares fit through the pitot thickness data at the aforementioned streamwise locations.

Table 5 shows that the growth rate of the primary shear layer is suppressed with addition of the secondary flow, a trend expected due to the increase of the velocity ratio U_s/U_p (decrease of the velocity difference) across this shear layer. At this point, we note a significant difference between the primary shear layer of a coaxial jet (where the secondary flow issues from an annular nozzle) from the shear layer of a single jet or the primary shear layer of "coflowing" jet, i.e., a jet surrounded by a very large secondary flow (such as a jet issuing inside a wind tunnel). In the coaxial case, the stream surrounding the primary shear layer is bounded by another shear layer (the secondary one) which exhibits instability and growth. In the single and coflowing cases, the outer stream is steady and virtually "unbounded". In other words, the primary shear layer of the coaxial case is not surrounded by "clean" conditions as in the single or coflowing jet. The same observation applies to the secondary shear layer whose inner stream is bounded by the unstable primary shear layer. Therefore, one expects to see some deviation in the growth rates δ'_p and δ'_s from those expected in the clean planar or axisymmetric cases.

It was of interest, therefore, to compare the growth

rates measured in our coaxial jets to the those predicted by the shear layer model described in the Introduction. One way of doing this is to compute the normalized growth rate δ'/δ'_0 and compare it to the compressibility correction curve of Eq. 4. This is done in Fig. 14 where we note the decline of the primary normalized growth rate with increasing M_c, consistent with the planar shear layer model, but also observe deviations from that model. The most significant deviation occurs for the lower-compressibility flow M90 whose growth rate is 20% to 40% higher than the model prediction, depending on nozzle diameter. The deviation is reduced with increasing secondary nozzle diameter, which suggests that the jet approaches the state of a "coflowing jet" that should be described well by the model. The secondary shear layer growth rates are lower than the model predictions and do not display a clear trend with increasing compressibility, although the range of M_c for the secondary shear layer was limited. Note that the measured shear layer growth rate for the SINGLE jet matches well the model prediction. These results suggest that accurate growth rate models for coaxial jets need to incorporate the interactions between the shear layers.

Model for the Potential Core Length

In this section we distill our data into models for the lengths of the primary and secondary potential cores of a coaxial jet. We start from two simple, clean flows: (a) the single jet and (b) the coflowing jet with primary flow same as the single jet and surrounded by a very large secondary flow. See Figs. 15(a) and (b). In both cases, the jet shear layer is surrounded by steady, well defined conditions and its growth rate should be well approximated by the planar shear layer model. Moreover, the growth rate is expected to be constant from the jet exit to just before the end of the potential core. It is reasonable, therefore, to approximate the potential core length as $L_p/D_p \sim 1/\delta'$ and use the growth rate model described in Eqs. 1 through 4 to predict δ'. Based on the growth rate and potential core length of case SINGLE, the constant of proportionality in the above relation is very close to 1.0. Therefore, we write $L_p/D_p = 1/\delta'$, where δ' is the pitot thickness growth rate. Specifically, the potential core length of the single jet is

$$\frac{L_{\text{SINGLE}}}{D_p} = \frac{1}{\delta'_{\text{SINGLE}}}$$

$$= \left[0.14(1+\sqrt{s})(0.23+0.77e^{-3.5M_c^2})\right]^{-1} \qquad (7)$$

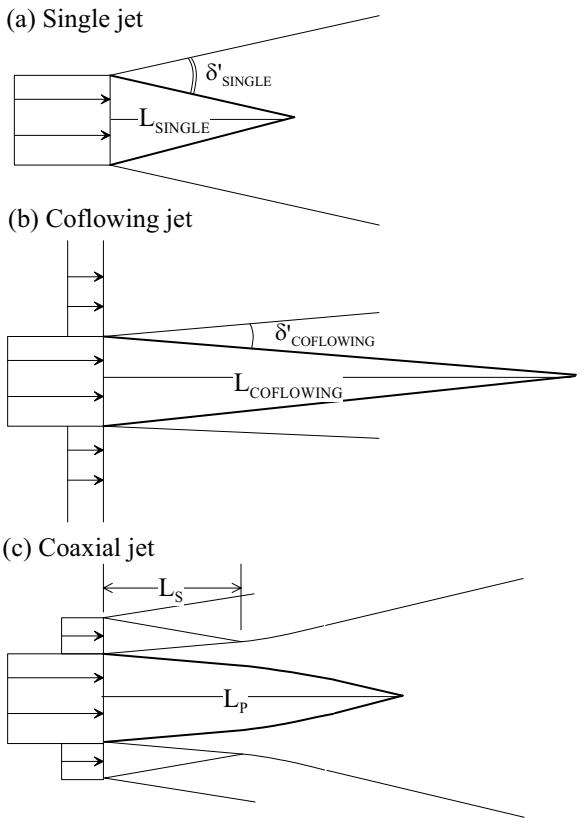

Fig.15 Potential core development in (a) single jet; (b) coflowing jet; and (c) coaxial jet.

where $s = \rho_p/\rho_\infty$ and $M_c = U_p/(a_p + a_\infty)$. The potential core length of the coflowing jet is

$$\frac{L_{\text{COFLOWING}}}{D_p} = \frac{1}{\delta'_{\text{COFLOWING}}}$$

$$= \left[0.14\frac{(1-r)(1+\sqrt{s})}{1+r\sqrt{s}}(0.23+0.77e^{-3.5M_c^2})\right]^{-1} \qquad (8)$$

where $r = U_s/U_p$, $s = \rho_s/\rho_p$, and $M_c = (U_p + U_s)/(a_p + a_s)$.

In the coaxial jet, Fig. 15(c), the secondary potential core is formed between the outer edge of the primary shear layer and the inner edge of the secondary shear layer. Its length is expected to be inversely proportional to the average growth rate of the surrounding shear layers,

$$\frac{L_s}{H} \sim \frac{2}{(\delta'_p + \delta'_s)} \qquad (9)$$

where H is the thickness of the secondary stream, $\delta'_p \approx \delta'_{\text{COFLOWING}}$ is given by Eq. 8, and δ'_s is given by

$$\delta'_s = 0.14(1+\sqrt{s})(0.23+0.77e^{-3.5M_c^2}) \qquad (10)$$

Table 5 Growth Rates

Case	M_{c_p}	δ'_p	$\delta'_p/\delta'_{p,0}$	M_{c_s}	δ'_s	$\delta'_s/\delta'_{s,0}$
SINGLE	0.68	0.106	0.414			
C14M37	0.48	0.067	0.456	0.18	0.150	0.539
C14M60	0.37	0.062	0.623	0.29	0.119	0.432
C14M90	0.23	0.071	1.318	0.43	0.146	0.541
C17M37	0.48	0.087	0.592	0.18	0.148	0.532
C17M60	0.37	0.071	0.714	0.29	0.136	0.494
C17M90	0.23	0.063	1.170	0.43	0.117	0.445
C20M37	0.48	0.078	0.518	0.18	0.125	0.449
C20M60	0.37	0.067	0.673	0.29	0.152	0.552
C20M90	0.23	0.065	1.112	0.43	0.135	0.500

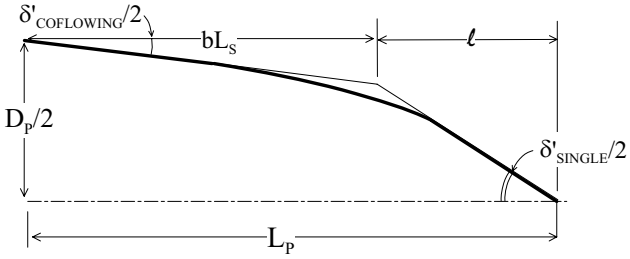

Fig.16 Geometric argument for the length of the primary potential core of a coaxial jet. Thick line describes the inner edge of the shear layer surrounding the potential core.

with $M_c = U_s/(a_s + a_\infty)$ and $s = \rho_s/\rho_\infty$. The proportionality constant of Eq. 9 was determined from the plot of Fig. 17 which presents the measured values of L_s/H plotted against the inverse of the sum of the model growth rates. A least-squares fit of the data yields

$$\frac{L_s}{H} = \frac{2.63}{(\delta'_{\text{COFLOWING}} + \delta'_s)} \tag{11}$$

This model predicts the secondary potential core lengths within 10% of their measured values.

Consider now a coaxial jet with secondary potential core shorter than the primary potential core. Initially, the growth rate of the primary shear layer is close to that of the coflowing jet. After the secondary potential core ends, the growth rate of the primary shear layer is expected to approach that of the single jet. We expect, therefore, the length of the primary potential core L_p to lie somewhere between L_{SINGLE} and $L_{\text{COFLOWING}}$ by an amount dependent on the length of the secondary potential core, L_s. Let us say that the determinant of this transition is bL_s, where b is a constant factor. Using the geometric argument of Fig. 16, $L_p = bL_s + \ell$ where

$$\ell = \frac{D_p}{\delta'_{\text{SINGLE}}} - \frac{\delta'_{\text{COFLOWING}}}{\delta'_{\text{SINGLE}}} bL_s \tag{12}$$

Replacing the growth rates by the corresponding potential core lengths per Eqs. 7 and 8, we obtain

$$\frac{L_p}{D_p} = \frac{L_{\text{SINGLE}}}{D_p} + \frac{bL_s}{D_p}\left(1 - \frac{L_{\text{SINGLE}}}{L_{\text{COFLOWING}}}\right) \tag{13}$$

We now correlate the measured values of L_p/D_p versus $(L_s/D_p)(1 - L_{\text{SINGLE}}/L_{\text{COFLOWING}})$. The plot of this correlation is shown in Fig. 18. A least-squares fit of the data gives

$$\frac{L_p}{D_p} = \frac{L_{\text{SINGLE}}}{D_p} + 2.1\frac{L_s}{D_p}\left(1 - \frac{L_{\text{SINGLE}}}{L_{\text{COFLOWING}}}\right) \tag{14}$$

which suggests that the transition from the coflowing-jet to the single-jet behavior ends at around $x = 2.1L_s$. This model predicts the potential core lengths within 10% of their measured values.

As the length of the secondary potential core L_s approaches the length of the primary potential core L_p, L_p should tend asymptotically to $L_{\text{COFLOWING}}$. This behavior is not incorporated in the present model and will be the subject of further research. For many practical situations, however, L_s is much shorter than L_p.

CONCLUDING REMARKS

Pitot pressure surveys have characterized the mean flow development of single and dual-stream air jets. Coaxial and eccentric dual-stream configurations have been explored. The effect of secondary-flow velocity and secondary-flow nozzle on the development

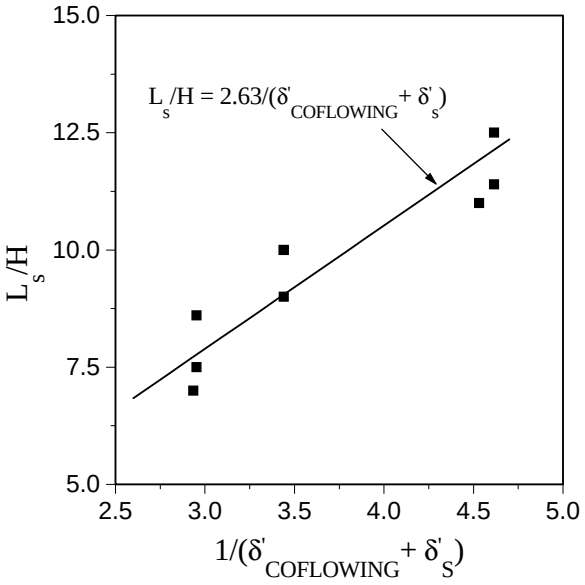

Fig.17 Model for the secondary potential core length of a coaxial jet.

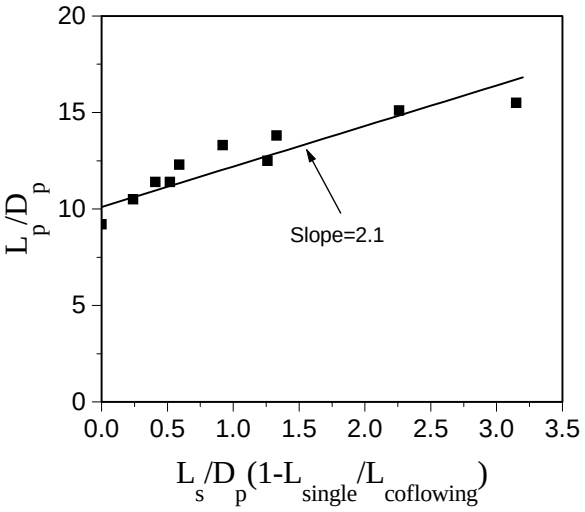

Fig.18 Model for the primary potential core length of a coaxial jet.

of the primary, Mach 1.5 flow is described, with special attention on the length of the primary potential core, the supersonic length of the plume, and the mass entrainment rate of the jet. In coaxial configurations, the primary potential core is elongated with increasing Mach number and/or increasing diameter of the secondary flow. For a Mach 0.9 secondary flow delivered from a nozzle with diameter ratio $D_s/D_p = 2.0$, the potential core is elongated by 68% relative to its value in the single jet. The length of the supersonic region is roughly proportional to the length of the primary potential core by the factor U_p/a_∞. Thus, the supersonic region is also elongated with addition of a secondary flow, a phenomenon that is undesirable from the perspective of noise.

The eccentric configuration exposes part of the primary jet to the ambient, thus allows the jet to grow at a faster rate than in the coaxial case. As a result, the potential-core and sonic lengths are elongated by a much smaller amount than in the coaxial case. This has an appreciable benefit on noise emission, especially when the secondary stream is used to prevent Mach wave formation. The entrainment rate of the eccentric jet is very close to that of the single jet when diameter of the secondary nozzle is $D_s/D_p = 1.4$. The eccentric jet was a convenient way to achieve an asymmetric dual-stream setup in our facility. It is not an optimal condition, yet it showed substantial benefit relative to the coaxial configurations. There is strong potential for more efficient asymmetric configurations, such as a round nozzle surrounded by a crescent-shaped secondary flow.

An approximate, empirical model for predicting the primary and secondary potential core lengths for a coaxial jet is proposed. It combines the present measurements of potential core lengths with the classical model of shear layer growth rate and gives predictions that are within 10% of the measured values.

Acknowledgments

The support by NASA Langley Research Center is gratefully acknowledged (Grant NAG-1-2104 monitored by Mr. Thomas D. Norum). We thank Mr. Sky Ellsworth for the construction of the pitot probe traverse system.

References

[1] Seiner, J.M., and Krejsa E., "Supersonic Jet Noise and the High Speed Civil Transport", AIAA-89-2358.

[2] Papamoschou, D., "Mach Wave Elimination in Supersonic Jets, " *AIAA Journal*, Vol. 35, No. 10, 1997, pp. 1604-1611.

[3] Papamoschou, D. and Debiasi, M., "Targeted Mach Wave Elimination," AIAA-2000-0085.

[4] Bishop, K.A., Ffowcs Williams, J.E., and Smith, W., "On the Noise Sources of the Unsuppressed High-Speed Jet," *Journal of Fluid Mechanics*, Vol. 50, Part 1, 1971, pp. 21-31.

[5] Forstall, W. Jr. and Shapiro, A.H., "Momentum and Mass Transfer in Coaxial Gas Jets," *Journal of Applied Mechanics*, Vol. 10, 1950, pp. 399-408.

[6] Ko, N.W.M. and Kwan, A.S.H., "The Initial Region of Subsonic Coaxial jets," *Journal of Fluid Mechanics*, Vol. 73, Part 2, 1976, pp. 305-332.

[7] Champagne, F.H. and Wygnanski, I.J., "An Experimental Investigation of Coaxial Turbulent Jets," *International Journal of Heat and Mass Transfer*, Vol. 14, 1971, pp. 1445-1464.

[8] Durao, D. and Whitelaw, J.H., "Turbulent Mixing in the Developing Region of Coaxial Jets," *Journal of Fluids Engineering*, Vol. 95, No. 3, 1973, pp. 467-473.

[9] Gladnick, P.G., Enotiadis, A.C., LaRue, J.C., and Samuelsen, G.S., "Near-Field Characteristics of a Turbulent Coflowing Jet," *AIAA Journal*, Vol. 28, No. 8, 1990, pp. 1405-1414.

[10] Williams, T.J., Ali, M.R.M.H., and Anderson, J.S., "Noise and Flow Characteristics of Coaxial Jets," *Journal of Mechanical Engineering Science*, Vol. 11, No. 2, 1969, pp. 133-142.

[11] Eggers, J.M. and Torrence, M.G., "An Experimental Investigation of the Mixing of Compressible-Air Jets in a Coaxial Configuration," NASA TN D-5315, 1969.

[12] Schadow, K.C., Gutmark, E., and Wilson, K.J., "Compressible Spreading Rates of Supersonic Coaxial Jets," *Experiments in Fluids*, Vol. 10, 1990, pp. 161-167.

[13] Papamoschou, D. and Roshko, A., "The Compressible Turbulent Shear Layer: An Experimental Study," *Journal of Fluid Mechanics*, Vol. 197, 1988, pp. 453-477.

[14] Goebel, S.G. and Dutton, J.C., "Experimental Study of Compressible Turbulent Mixing Layers," *AIAA Journal*, Vol. 29, No. 4, 1991, pp. 538-546.

[15] Elliott, G.S., Samimy, M., and Arnette, S.A., "The Characteristics and Evolution of Large-Scale structures in Compressible Mixing Layers," *Physics of Fluids*, Vol. 7, No. 4, 1995, pp. 864-876.

[16] Hall, J.L., Dimotakis, P.E., and Rosemann, H., "Experiments in Nonreacting Compressible Shear Layers," *AIAA Journal*, Vol. 31, No. 12, 1993, pp. 2247-2254.